Raman Spectroscopy of Mackinawite FeS in Anodic Iron Sulfide Corrosion Products

Georgi Genchev[a,c] and Andreas Erbe[a,b,z]

[a]*Max-Planck-Institut für Eisenforschung GmbH, 40237 Düsseldorf, Germany*
[b]*Department of Materials Science and Engineering, NTNU - Norwegian University of Science and Technology, 7491 Trondheim, Norway*

Raman spectroscopy in a confocal microscope was used to study electrochemically synthesized corrosion products from sour gas experiments. When exposed to oxygen-containing atmosphere, the initial mackinawite FeS corrosion product transformed under laser irradiation to hematite, Fe_2O_3. Measurements with a thin water layer on top of the corrosion products prevented the transformation, as drying was prevented. In situ Raman measurements of mackinawite formation avoided the problem of transformation completely. In situ and operando, the initially formed mackinawite showed two Raman peaks in the wavenumber range >180 cm^{-1} centered around 200–215 cm^{-1} and 285–300 cm^{-1}. On an empirical basis, these modes were assigned to a B_{1g} mode of the iron sublattice and an A_{1g} mode of the sulfur sublattice, respectively. A comparison with a literature assignment for aged mackinawite suggests that the aging observed involves significant changes in the sulfur sublattice.
 [DOI: 10.1149/2.1151606jes] All rights reserved.

Manuscript submitted February 15, 2016; revised manuscript received March 15, 2016. Published March 25, 2016.

Corrosion of iron in H_2S containing solutions is a general problem in crude oil and natural gas production, and is generally referred to as sour corrosion. Aqueous H_2S solutions promote corrosion of steels,[1–3] but the exact nature and mechanisms of corrosion strongly depend on the reaction conditions.[4–7] While the process has been widely investigated for pure iron,[8–12] and carbon steels,[13–17] there is still a lack of understanding of the reaction path and electronic properties of the corrosion products.[18,19]

The chemistry of the corrosion products formed during H_2S-triggered corrosion is rather complex, as there are many different solids consisting only of iron and sulfur.[20] However, mackinawite has been found to be the initial,[8,21] and probably most important corrosion product, of iron in aqueous sulfide solutions as it was observed in reactions carried out over a wide range of pH and temperature.[11,19,22–24] It possesses a tetragonal, layered crystal structure,[25–27] and can be synthesized by precipitation from solutions containing Fe^{2+} and S^{2-} solutions,[28,29] or by reaction of sulfide solution with metallic iron.[19,21,26,30] In the field of microbially induced corrosion, sulfate-reducing bacteria are known to transform sulfate compounds into iron sulfides, e.g. mackinawite.[31–36]

Raman spectroscopy has become an important tool for identification of corrosion products.[37–45] Some major problems may still occur due to laser heating, fluorescence, or low sensitivity as a consequence of the small cross-sections of Raman scattering. However, the fact that glass and water are both very weak Raman scatterers makes this technique suitable for in situ measurements in aqueous environments.[46–48] The presence of water has an additional positive effect on the process as it decreases the heating from the laser. The use of (in situ and operando) Raman spectroscopy for study corrosion process studies of iron in sulfide rich environments has been already reported.[29,49] In previous work,[19] Raman spectroscopy was used to confirm the nature of iron sulfide films obtained as corrosion products from polarization experiments. Collected spectra showed a good agreement with the database Raman spectrum of mackinawite,[19,50] but distinct disagreement with data from other authors was found.[29,49,51,52] Due to the lack of availability of a normal mode analysis for mackinawite, no detailed interpretation of the Raman data was possible. Recently, a study by density functional theory (DFT) became available, which reported computed vibrational spectra of mackinawite.[53]

In this work, corrosion products from sour gas experiments were synthesized using in situ potentiostatic polarization experiments. Potentials above the initial corrosion potential, E_{corr}, were applied in order to enhance the anodic reactions. In the course of the experiments, corrosion products were studied in situ (state of formation) and ex situ (wet or dry samples exposed to air). For iron oxides, which strongly absorb light, it is well known that heat-induced transformations may be observed during Raman experiments.[54–56] Iron sulfide corrosion products are also strong light absorbers,[19] which motivates a closer comparison between ex situ and in situ results, especially in the view of the above-mentioned disagreement of spectra between different sources. Special emphasis is placed on the discussion of spectral changes during oxidation of the corrosion products. Furthermore, for oxide thin films it is known that in situ characterization sometimes leads to different results than post mortem analysis.[57,58]

Experimental

Experiments were performed on 99.8% pure iron. The used metal coupons had dimensions of 2.0 cm × 2.0 cm × 0.1 cm and were ground with 320 SiC paper prior to each experiment. To remove organic contaminations, the surface was subsequently cleaned with water and methanol, and dried under a nitrogen stream.

The electrochemical experiments used in this work to generate corrosion product layers were conducted in NACE Test Solution A.[59] The solution contained analytical grade sodium chloride (5 wt%) and glacial acetic acid (0.5 wt%), both purchased from Merck. The electrolyte was prepared using water with a conductivity of <0.055 μS cm^{-1} from an USF ELGA (Ransbach-Baumbach, Germany) Purelab Plus UV water purification system. The pH of the solution before contact with the metal specimen was measured to be 2.6. Gaseous H_2S (Air Liquide, Düsseldorf, Germany) with purity of 99.5% was used (max. impurities: 500 ppm-vol CO_2, N_2, CH_4, CS_2; 3000 ppm-vol COS). The used N_2 was of high purity grade (>99.9%).

Ex situ investigations.—Samples for the ex situ investigations were prepared in an air tight homebuilt flat bottom PMMA cell of 500 mL electrolyte volume and electrode area $A = 0.785$ cm^2. The electrolyte was first de-oxygenated by purging with nitrogen, and then saturated with hydrogen sulfide for at least 30 min. H_2S purging was maintained throughout the experiments to minimize ingress of oxygen. The conditions used were similar to those reported elsewhere.[19] Polarization and ex situ spectroscopy were conducted at room temperature. No stirring was applied during polarization.

[c]Present Address: Salzgitter Mannesmann Forschung GmbH, 47259 Duisburg, Germany.
[z]E-mail: a.erbe@mpie.de; aerbe@arcor.de

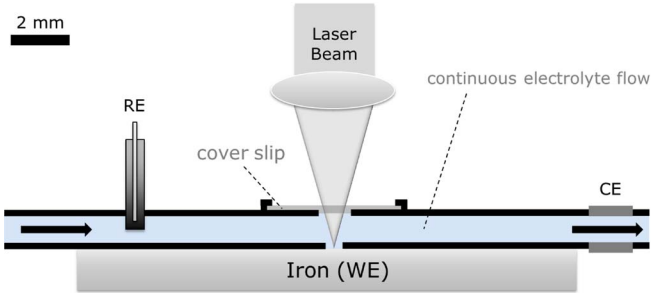

Figure 1. Scheme of electrochemical cell used for in situ Raman measurements (cell thickness 1 mm; cover slip thickness 0.2 mm; tubing diameter 0.6 mm; electrode area 0.2 cm^2).

For ex situ Raman measurements, potentiostatic polarization at 200 mV above the initial corrosion potential was used for the preparation of sulfide films on the surface of the iron sample. The total reaction time was 44 h. For this purpose, a typical three-electrode arrangement and a Gamry PCIV/Series G Family potentiostat (Gamry Instruments Inc.) were used. A carbon rod (Mueller and Roessner, Troisdorf, Germany) acted as the counter electrode, and a commercial Ag/AgCl/3M KCl as reference electrode (Metrohm, Filderstadt, Germany). Using a Luggin capillary arrangement, the reference electrode was positioned very close to the iron sample serving as working electrode.

In situ experiments.—For the in situ experiments, the used setup was modified to fit under a confocal Raman microscope, which led to a cell with significantly smaller dimensions (Fig. 1, $A = 0.2$ cm^2). Because of safety concerns, H_2S-prepurged solutions were used for in situ experiments. However, N_2 purging was maintained throughout the experiments to minimize ingress of oxygen. Because of the small size of the cell and the connecting pipes, a lower potential (50 mV above E_{corr}) was applied to produce the iron sulfide layers. In this way, excessive formation of bubbles at the counter electrode because of hydrogen evolution and a subsequent plugging of the tubing was avoided. A peristaltic pump was used, thus allowing circulation of the test electrolyte, starting with H_2S-free solution and then switching to H_2S-saturated electrolyte. Continuous flow over the iron was maintained throughout the experiments. In this way, the surface was cooled, preventing a laser-induced heating of the surface. The total reaction time was 30 min. As the size of the in situ Raman cell was small, a modified three-electrode arrangement for the electrochemical experiments was used, with a carbon rod (Mueller and Roessner, Troisdorf, Germany) as the counter electrode, a commercial Ag/AgCl/3M KCl as reference electrode (Metrohm, Filderstadt, Germany), and the iron sample as working electrode. A Gamry PCIV/Series G Family (Gamry Instruments Inc.) potentiostat was used. A Luggin capillary arrangement was used to protect the reference electrode from getting poisoned by sulfide species.

Raman spectra were recorded on an alpha300M confocal Raman microscope (WiTec, Ulm, Germany), with an excitation wavelength of 532.1 nm. Illumination and detection was performed through a microscope objective of 100× magnification, numerical aperture of 0.75 for ex situ, and of 40× magnification, numerical aperture of 0.6 for in situ experiments. Ex situ spectra were recorded in ambient air atmosphere without special protection. The resulting spectra were analyzed using the WiTec Project software.

The identification of the ex situ products using grazing incidence X-ray diffraction (GI-XRD) was conducted on a Bruker D8 Advance diffractometer with Cu K_α radiation and a Sol-X solid-state detector. Diffraction patterns were collected at an angle of incidence $\alpha = 3^\circ$ within a range of the scattering angle 2θ of $10^\circ < 2\theta < 75^\circ$ in steps of 0.05°, and an integration time of 60 s per step. XRD patterns were evaluated using the DIFFRACplus EVA package.

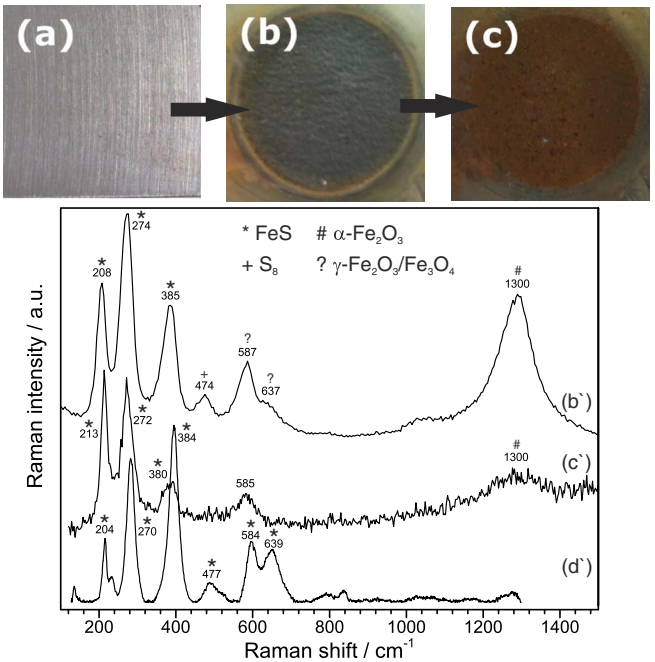

Figure 2. (a) The bare metal before exposure to saline H_2S saturated acetic solution. (b) Image of area of exposure after anodic polarization for 44 h at 200 mV above E_{corr} and (b′) the corresponding Raman spectrum. (c) Image of corrosion products after aging in air for 90 d and (c′) the corresponding Raman spectrum. (d′) Reference Raman spectrum for mackinawite as found in the RRUFF database.[50] In the spectra, peaks have been assigned by symbols to certain substances, see Table I. The assignment to FeS is based on the RRUFF database,[50] and is in disagreement with some sources.[29,51,52]

Results and Discussion

The coverage of the metal sample with a black precipitate was indicative of the successful growth of corrosion products film containing iron sulfide compounds. The formation of iron sulfides in H_2S-saturated solutions using electrochemical techniques is well known.[8,19,21,49,60]

Under the conditions used in this work, formation of a black layer of corrosion products on top of the metal surface was already observed after several hours. In Fig. 2, the well-formed FeS layer after a reaction time of 44 h is depicted. (SEM images of similar corrosion product layers are available elsewhere.[19]) The Raman spectrum of the sample after drying with water/alcohol in a nitrogen stream (Fig. 2b′) is in good agreement with literature spectra attributed to the iron sulfide mackinawite, e.g., spectrum (d′) in Fig. 2.[29,52,53] Moreover, XRD measurements showed that mackinawite is the only detectable crystalline compound in the obtained corrosion products (Fig. 3b). After aging the products in air (in this example for 90 days), a change in their color from black to rust-red became visible (Fig. 2c). This is a clear indication for the oxidation of the initial products and has been supported by XRD measurements (Fig. 3c), which confirmed the presence of the iron(III) oxide hydroxide phase akaganeite.

The corresponding Raman spectrum of the oxidized compound (Fig. 2c′) looked, however, almost identical to the spectrum of the non-oxidized compound, mackinawite. Further, the spectrum does not match the one for akaganeite, but rather the one for hematite.[50,54,55] A possible explanation for these observations is a transformation of the compound during the Raman measurements, e.g. as a consequence of heating by laser light absorption in the presence of oxygen from air. Hematite was found also in other works as the result of laser heating.[54,61] Hematite has an intense spectrum characterized by the strong resonant band at 1310 cm^{-1} under green excitation.[61] Further Raman experiments have been conducted with dry samples. These samples were protected with Capton foil from air. Laser exposure was

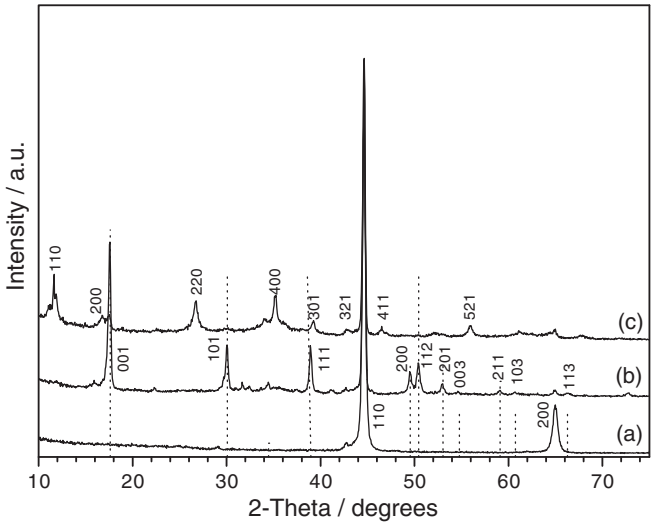

Figure 3. GI-XRD patterns of (a) the bare metal (pure iron; JCPDF no. 06-0696) before exposure to the saline H_2S saturated acetic solution, (b) the electrochemically grown corrosion products (mackinawite; JCPDF no. 15-0037), including lines showing position and relative intensities based on JCPDF no.15-0037 for mackinawite, and (c) the corrosion products after exposure to air for 90 d (akaganeite; JCPDF no. 34-1266).

minimized to a power of typically several hundreds of μW, but always below 1 mW (corresponding to $\approx 6 \cdot 10^9$ W m^2 around the focus of the objective). As a result, however, always the same Raman spectrum as shown in Fig. 2c′ was observed.

In order to identify the reaction products correctly, in situ experiments have been conducted. This approach has been successfully used by other groups.[29,49] The advantages of in situ techniques are the possibility to monitor the corrosion products in their state of formation,[62] but also to avoid the contact of the sample with oxygen due to post-preparation work, transport, etc. The in situ cell shown in Fig. 1 was used for these experiments. The peristaltic pump allowed circulation of the test solution. The maintaining of the continuous flow over the iron was crucial in order to keep the surface cooled, thus preventing laser-induced heating of the surface. Moreover, due to the purging of the electrolyte with N_2 throughout the in situ experiment, the ingress of oxygen in the cell was reduced to a minimum.

The observed visual changes of the surface during the in situ experiments and the collected Raman spectra are depicted in Fig. 4. The corresponding current time curve recorded during the experiment is shown in Fig. 5, together with the corresponding curve for the preparation of the samples for ex situ experiments (inset). Formation of black corrosion products was observed almost immediately after starting the electrode polarization (Fig. 4c). The only significant Raman bands were observed at 286 cm^{-1} and 202 cm^{-1} in the example shown (Fig. 4c′), indicating the formation of mackinawite.[29,49] No additional bands were detected after polarization for up to 30 min and total exposure to the electrolyte of up to 3 h at E_{corr}. After terminating the electrochemical experiment, the position of the sample was shifted to illuminate a different area of the surface. The collected Raman spectra confirmed the uniform coverage of the surface by the iron sulfide mackinawite. However, removing the sample from the cell and drying in a nitrogen stream lead to a change of the spectrum. The detected Raman bands after drying were also in good agreement with those of the iron(III) oxide hematite.[50,61] Dominant Raman peaks of the different relevant iron compounds are summarized and compared to literature values in Table I.

Using the information from the in situ measurements, another simpler experiment was developed. For this experiment, the sample was just taken out of the electrochemical cell after a regular polarization experiment, and was carefully washed with distilled water. Care was taken not to remove the thin water layer on top of the reaction products.

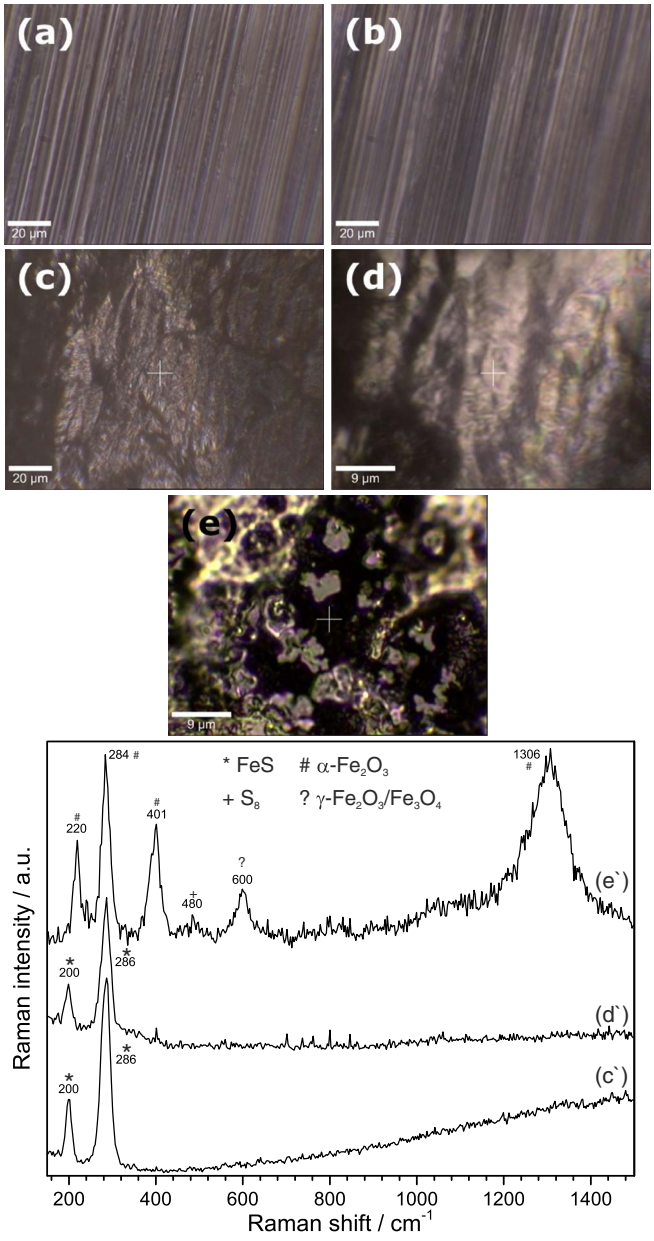

Figure 4. Results from in situ Raman experiments. (a), (b) Microscopic images recorded in the same confocal microscope as used for the Raman measurements of the surface before and after introducing the H_2S saturated electrolyte, respectively. (c) Image of substrate surface after starting the electrochemical treatment and (c′) corresponding Raman spectrum. Current time transients during polarization are shown in Fig. 5. (d) Image of surface after termination of the polarization and (d′) corresponding Raman spectrum. (e) Image of corrosion products after removing from in situ cell and drying with nitrogen stream and (e′) corresponding Raman spectrum.

Subsequently, Raman measurements were conducted. Raman spectra obtained in this configuration agree well with spectra of the in situ experiments (Fig. 6). The iron sulfide corrosion products appeared stable and close to their initial structure under the the thin water film. During the evaporation of the water layer in ambient atmosphere, further Raman spectra showed transformation of the compound to hematite (as shown in the ex situ experiments above), but with magnetite as an intermediate (Fig. 6).

The different routes of oxidation observed here are summarized in Fig. 7. In the sulfide containing electrolyte, iron was oxidized to FeS (reaction 1). Both Raman and XRD showed the presence of

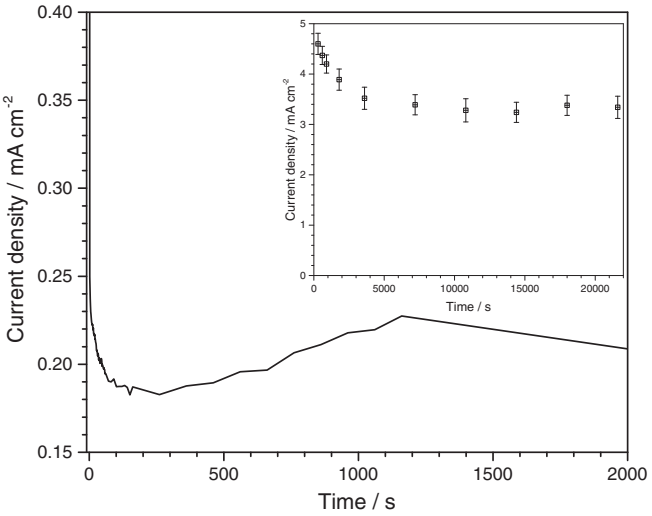

Figure 5. Time dependence of current densities during potentiostatically controlled growth of a corrosion product layer in an in situ Raman experiment. Polarization was carried out 50 mV above E_{corr}. The recorded Raman spectra are depicted in Fig. 4. Inset: Corresponding current time curves for polarization of samples for ex situ Raman experiments, where polarization was carried out 200 mV above E_{corr}. A discussion of current time transients is available elsewhere.[19]

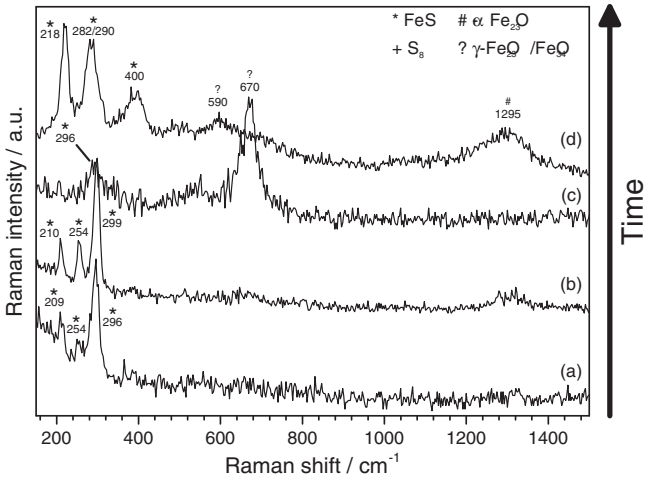

Figure 6. Results from ex situ Raman experiments of a sample with thin water layer on top. Sample were dried "naturally" by evaporation of water during the recording of spectra. (a) The Raman bands at 209 cm^{-1} and 296 cm^{-1} show the presence of FeS (mackinawite) of the wet sample. (b) An additional band at 253 cm^{-1} arouse when water layer became thinner. (c) A strong band at 671 cm^{-1} indicates the transformation of the initial corrosion product mackinawite to magnetite, Fe_3O_4). (d) The final transformation product hematite (219 cm^{-1}, 285 cm^{-1}, 396 cm^{-1}, 1306 cm^{-1}) was detected when sample was completely dry, similar to results of ex situ experiments.

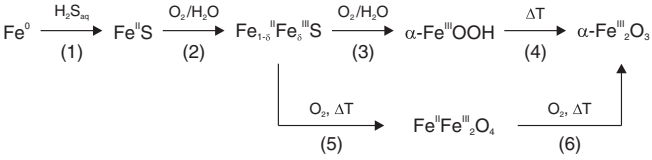

Figure 7. Scheme summarizing the observed chemical transformations. During exposure to H_2S-containing electrolyte (1), iron transformed into mackinawite FeS. Partial oxidation (2) led to a mixed sulfide. Different further oxidation was observed depending on whether the process was carried out in presence of water (3, 4) or in absence of macroscopic amounts of water (5, 6). ΔT indicates heating, in this particular case as a consequence of exposure to a laser source.

tetragonal mackinawite. Peak shifts in the Raman spectrum observed after exposure to oxygen have been interpreted as indication of a partial further oxidation of the initially formed mackinawite to a product containing a fraction of Fe^{III} (reaction 2).[29,51,52] From here onward, further oxidation was different depending on whether it took place in the presence or absence of a thin electrolyte film. In the presence of an electrolyte film, the iron(III) oxide hydroxide akaganeite, FeOOH, formed during exposure to air (reaction 3), which transformed by laser heating to hematite, Fe_2O_3 (reaction 4). In the absence of an electrolyte film, laser heating decomposed the sulfide into magnetite, Fe_3O_4 (reaction 5). Fe_3O_4 was completely oxidized by further laser heating into hematite (reaction 6 in Fig. 7). Results are in agreement with previous reports on oxidation of iron sulfides.[29,63]

The Raman spectrum of the primary corrosion product mackinawite can be analyzed in detail. This spectrum consists of two peaks in the spectral range investigated here, in line with previous reports.[29,53] Tetragonal FeS forms a layer structure in which the iron atoms are arranged in centered squares, and the sulfur atoms lie alternately above and below the layers.[25,27,64–66] Each sulfur atom is surrounded by four nearest iron atoms, resulting in a square-based pyramid coordination polyhedron. The space group is *P4/nmm* with the unit cell containing two formula units of FeS.[25,27,64–66] For a unit cell containing 4 atoms, as in case of mackinawite, 12 vibrations are expected in total. The Fe atoms lie on D_{2d} sites (Wyckoff position 2a) and give rise to two Raman active modes: B_{1g} and E_g. The sulfur atoms occupy C_{4v} sites (Wyckoff position 2c) and also give rise to two Raman active vibrations: A_{1g} and E_g. Overall, four different modes are Raman active with respect to the above mentioned space group: A_{1g}, B_{1g}, and 2 E_g modes.[53,67–69] For "aged", polycrystalline mackinawite developed after two months exposure, these have been assigned on the basis of

Table I. Reported Raman peak positions for mackinawite and other relevant iron phases compared to values found in this work.

Compound	Composition	Position / cm^{-1}	Ref.
Mackinawite	FeS	200, (253), 287	This work, in situ
Mackinawite	FeS	212, 298	This work, ex situ
Nanocryst. mackinawite	FeS	208, (256), 283	29
Cryst. mackinawite	FeS	208, 257, 298	29
Amorph. mackinawite	FeS	208, 282	49
Amorph. mackinawite	FeS	214, 282	75
Hematite	Fe_2O_3	218, 285, 401, 1306	This work
Hematite	Fe_2O_3	223, 289, 404, 1310	61,76
Maghemite	Fe_2O_3	377, 510, 670, 715	77
Akaganeite	FeOOH	310, 390, 720	61,76
Magnetite	Fe_3O_4	671	This work
Magnetite	Fe_3O_4	671	61,76
Elemental sulfur	S_8	153, 219, 472	78

DFT calculation as 388 cm^{-1}, 225 cm^{-1}, 243 cm^{-1}, and 396 cm^{-1}, respectively.[53] On the other hand, the observation in this work is that XRD already shows a typically crystalline mackinawite diffraction pattern, even though the Raman spectrum is similar to the spectrum that other sources assigned to a special nanocrystalline "initial" form of mackinawite.[29,52,53] It is not directly obvious why a nanocrystalline mackinawite should have a Raman spectrum that is so qualitatively different from the spectrum of the crystalline product. The fact remains that the observed Raman spectra for the "initial" mackinawite contains only two of the four modes expected (Table I). The two missing modes may be below the accessible wavenumber range. At lower wavenumbers, the spectrum of water complicates the analysis. However, compared to the spectra of "aged" mackinawite,[53] the modes should actually be in the spectral range investigated here.

For an interpretation of the Raman spectrum of "initial" mackinawite, a comparison with other compounds in spacegroup *P4/nmm* is instructive, in addition to a comparison to the calculated spectrum for "aged" mackinawite.[53] Raman studies of thin films of SnO,[68] and single crystals of both FeTe[70] and FeSe[71] show the absence of the E_g modes because of crystal orientation. (On the other hand, the E_g modes were detected e.g. in PbO and FeS in appropriate experiments.[53,69]) Layers of mackinawite corrosion products are often strongly textured in (001) direction as well.[19] We therefore conclude that the E_g modes are absent here as well due to texturing,[68] so that the dominant modes at 200–215 cm^{-1} and 285–300 cm^{-1} must be A_{1g} and B_{1g} mode. The small peak at 258 cm^{-1} visible in the spectra in Figs. 6a and 6b may originate from one of the E_g modes, as these films are not single crystalline. Such an assignment agrees with DFT calculations.[53] In "aged" mackinawite,[53] as well as in iron compounds that crystallize in the same space group, FeTe,[70] FeSe,[71] and both LaFeAsO and SmFeAsO,[72] B_{1g} modes of the Fe sublattice at the Wyckoff position 2a are observed between 190 and 230 cm^{-1}, which agrees with one of the peaks observed for the "initial" mackinawite investigated in this study. We therefore reason that the peak at 200–215 cm^{-1} corresponds to the B_{1g} mode of the Fe sublattice in "initial" mackinawite FeS. Consequently, the mode at 286 cm^{-1} should be the A_{1g} mode of the S sublattice. This assignment is not in agreement with the assignment based on DFT calculations for "aged" mackinawite, which reports the A_{1g} mode of the S sublattice around 380 cm^{-1}.[53] (Aged mackinawite shows no peak around 286 cm^{-1}). Both assignments are reasonable when compared to the modes of the chalcogenide sublattices in FeTe (159 cm^{-1}),[70] and FeSe (180 cm^{-1}),[72] which follow the expected trends based on the atomic masses of Te, Se, and S.

The evolution of the spectrum of mackinawite and mackinawite-like corrosion products with time,[29,53] together with the assignments as far as they agree between "initial" and "aged" mackinawite, may serve as a starting point to discuss in more detail the structural evolution of mackinawite corrosion products. "Aged" mackinawite is polycrystalline and shows both E_g modes. These modes are absent in the strongly textured "initial" mackinawite. The characteristic B_{1g} mode of the Fe sublattice changes slightly in position, which may be attributed to partial oxidation with time.[29,51,52] If the reasoning in the previous paragraph is correct, strong restructuring occurs in the S sublattice of mackinawite over time.

It is known from other compounds, e.g. ZnO,[73,74] that point defects, e.g. vacancies, can significantly alter the Raman spectrum. The frequencies from the DFT calculation of Raman-inactive modes do not suggest that an otherwise Raman-inactive mode becomes Raman active in the "initial" mackinawite.[53] Defect curing or formation within the S-sublattice (e.g. as a side product of partial oxidation) may therefore be one possible reason for the observed strong peak shift. In a previous work, the initial corrosion products have been shown to be oxygen-rich, even though XRD showed mackinawite as the only crystalline corrosion product.[19] An oxygen-rich partial lattice should cause a shift of the B_{1g} mode to even higher frequencies, as oxygen is lighter than sulfur. On the other hand, such an interpretation contradicts the DFT-based interpretation of spectra for "aged" mackinawite.[53] A systematic comparison of DFT calculations for tetragonal FeTe, FeSe and FeS with a common underlying approach has been suggested as one step to further the understanding of the spectra,[53] and may indeed be needed. On the experimental side, polarization-dependent measurements (which require special precautions for in situ cell design) should contribute to the understanding of the FeS evolution.

Conclusions

In ambient atmosphere, iron sulfide corrosion products underwent oxidation to iron oxides and subsequently suffered the heat induced transformations known from Raman spectroscopy of iron oxides (Fig. 7). Apparently, some spectra reported in the literature and in reference databases were affected by this problem and present therefore mixed spectra including iron oxide peaks. Consequently, different sources report different Raman spectra for the same compound, in this case mackinawite FeS. Even reported reference spectra need to be treated carefully. Because the peaks of A_{1g} and one E_g mode of hematite are very close to the B_{1g} and A_{1g} modes of "initial" mackinawite, hematite may be wrongly identified as mackinawite. Oxidation and subsequent transformation can be avoided either by in situ experiments, or by a simple wetting of the sample with water, and ensuring a thin water film remains present during the Raman measurement.

Comparing results from this work to literature data[53] shows that the spectrum of mackinawite itself significantly changes with time if the mackinawite-based corrosion products are exposed to sulfide-containing media. The different spectra observed over time in the literature may be explained by restructuring, defect healing and defect formation within the sulfur sublattice, possible caused by minor oxidation of a fraction of the Fe^{II} in mackinawite. The observed aging clearly does imply structural changes on the local level. Overall, this work serves as an example that post mortem analysis of corrosion products is sometimes not sufficient for a full understanding of the corrosion process.

Acknowledgment

The authors thank Salzgitter Mannesmann Forschung GmbH (SZMF) for funding this collaborative research project, C. Bosch of SZMF for helpful discussions, Prof. M. Stratmann for his continuous support, Petra Ebbinghaus for technical assistance and the MPIE mechanical workshop for building the in situ cell.

References

1. D. R. Morris, L. P. Sampaleanu, and D. N. Veysey, *J. Electrochem. Soc.*, **127**, 1228 (1980).
2. D. MacDonald, J. Begley, J. Bockris, J. Kruger, F. Mansfeld, P. Rhodes, and R. Staehle, *Mater. Sci. Eng.*, **50**, 19 (1981).
3. D. Ifezue and V. Nettikaden, *J. Fail. Anal. Preven.*, **13**, 264 (2013).
4. S. Nešić, *Corros. Sci.*, **49**, 4308 (2007).
5. M. S. Wiener, B. V. Salas, M. Quintero-Núñez, and R. Zlatev, *Corros. Eng. Sci. Technol.*, **41**, 221 (2006).
6. E. Sosa, R. Cabrera-Sierra, I. García, M. T. Oropeza, and I. González, *Corros. Sci.*, **44**, 1515 (2002).
7. J. Bana, U. Lelek-Borkowska, B. Mazurkiewicz, and W. Solarski, *Electrochim. Acta*, **52**, 5704 (2007).
8. D. W. Shoesmith, M. G. Bailey, and B. Ikeda, *Electrochim. Acta*, **23**, 1329 (1978).
9. H. Y. Ma, X. L. Cheng, S. H. Chen, G. Q. Li, X. Chen, S. B. Lei, and H. Q. Yang, *Corrosion (Houston, TX, U.S.)*, **54**, 634 (1998).
10. H. Ma, X. Cheng, S. Chen, C. Wang, J. Zhang, and H. Yang, *J. Electroanal. Chem.*, **451**, 11 (1998).
11. H. Ma, X. Cheng, G. Li, S. Chen, Z. Quan, S. Zhao, and L. Niu, *Corros. Sci.*, **42**, 1669 (2000).
12. E. Abelev, T. A. Ramanarayanan, and S. L. Bernasek, *J. Electrochem. Soc.*, **156**, C331 (2009).
13. S. Arzola, J. Mendoza-Flores, R. Duran-Romero, and J. Genesca, *Corrosion (Houston, TX, U.S.)*, **62**, 433 (2006).
14. N. Sridhar, D. S. Dunn, A. M. Anderko, M. M. Lencka, and U. Schutt, *Corrosion (Houston, TX, U.S.)*, **57**, 221 (2001).
15. S. Papavinasam, R. W. Revie, M. Attard, A. Demoz, and K. Michaelian, *Corrosion (Houston, TX, U.S.)*, **59**, 897 (2003).

16. L. A. C. J. Garcia, C. J. B. M. Joia, E. M. Cardoso, and O. R. Mattos, *Electrochim. Acta*, **46**, 3879 (2001).
17. E. Sosa, R. Cabrera-Sierra, M. T. Oropeza, F. Hernández, N. Casillas, R. Tremont, C. Cabrera, and I. González, *Electrochim. Acta*, **48**, 1665 (2003).
18. W. Sun and S. Nesic, *NACE - Int. Corros. Conf. Ser.*, 07655 (2007).
19. G. Genchev, K. Cox, T. H. Tran, A. Sarfraz, C. Bosch, M. Spiegel, and A. Erbe, *Corros. Sci.*, **98**, 725 (2015).
20. D. Rickard and G. W. Luther, *Chem. Rev.*, **107**, 514 (2007).
21. D. W. Shoesmith, P. Taylor, M. G. Bailey, and D. G. Owen, *J. Electrochem. Soc.*, **127**, 1007 (1980).
22. H. Vedage, T. Ramanarayanan, J. Mumford, and S. Smith, *Corrosion (Houston, TX, U.S.)*, **49**, 114 (1993).
23. R. Cabrera-Sierra, M. Miranda-Hernández, E. Sosa, T. Oropeza, and I. González, *Corros. Sci.*, **43**, 2305 (2001).
24. C. Zhou, X. Chen, Z. Wang, S. Zheng, X. Li, and L. Zhang, *Corros. Sci.*, **89**, 30 (2014).
25. R. A. Berner, *Science*, **137**, 669 (1962).
26. R. A. Berner, *J. Geol.*, **72**, 293 (1964).
27. A. R. Lennie, S. A. T. Redfern, P. F. Schofield, and D. J. Vaughan, *Mineral. Mag.*, **59**, 677 (1995).
28. M. Wolthers, S. J. Van der Gaast, and D. Rickard, *Am. Mineral.*, **88**, 2007 (2003).
29. J. A. Bourdoiseau, M. Jeannin, R. Sabot, C. Rémazeilles, and P. Refait, *Corros. Sci.*, **50**, 3247 (2008).
30. A. Hernandez-Espejel, M. Palomar-Pardave, R. Cabrera-Sierra, M. Romero-Romo, M. T. Ramirez-Silva, and E. M. Arce-Estrada, *J. Phys. Chem. B*, **115**, 1833 (2011).
31. G. Chen and C. R. Clayton, *J. Electrochem. Soc.*, **144**, 3140 (1997).
32. P. Refait, D. D. Nguyen, M. Jeannin, S. Sable, M. Langumier, and R. Sabot, *Electrochim. Acta*, **56**, 6481 (2011).
33. D. Enning, H. Venzlaff, J. Garrelfs, H. T. Dinh, V. Meyer, K. Mayrhofer, A. W. Hassel, M. Stratmann, and F. Widdel, *Environ. Microbiol.*, **14**, 1772 (2012).
34. P. Beese, H. Venzlaff, J. Srinivasan, J. Garrelfs, M. Stratmann, and K. J. Mayrhofer, *Electrochim. Acta*, **105**, 239 (2013).
35. P. F. Beese-Vasbender, S. Nayak, A. Erbe, M. Stratmann, and K. J. Mayrhofer, *Electrochim. Acta*, **167**, 321 (2015).
36. Y. El Mendili, A. Abdelouas, and J.-F. Bardeau, *Phys. Chem. Chem. Phys.*, **15**, 9197 (2013).
37. A. Hugot-Le Goff and C. Pallotta, *J. Electrochem. Soc.*, **132**, 2805 (1985).
38. A. Hugot-Le Goff, J. Flis, N. Boucherit, S. Joiret, and J. Wilinski, *J. Electrochem. Soc.*, **137**, 2684 (1990).
39. C. A. Melendres, J. Acho, and R. L. Knight, *J. Electrochem. Soc.*, **138**, 877 (1991).
40. L. J. Simpson and C. A. Melendres, *J. Electrochem. Soc.*, **143**, 2146 (1996).
41. L. J. Oblonsky, S. Virtanen, V. Schroeder, and T. M. Devine, *J. Electrochem. Soc.*, **144**, 1604 (1997).
42. J. E. Maslar, W. S. Hurst, W. J. Bowers, J. H. Hendricks, and M. I. Aquino, *J. Electrochem. Soc.*, **147**, 2532 (2000).
43. J. M. Smith, J. C. Wren, M. Odziemkowski, and D. W. Shoesmith, *J. Electrochem. Soc.*, **154**, C431 (2007).
44. P. Vandenabeele, H. G. M. Edwards, and L. Moens, *Chem. Rev.*, **107**, 675 (2007).
45. M. Musiani, J.-Y. Liu, and Z.-Q. Tian, Applications of electrochemical surface-enhanced Raman spectroscopy (EC-SERS). In *Developments in Electrochemistry*, pp. 137–162. Wiley, Chichester, UK (2014).
46. V. Tolstoy, I. Chernyshova, and V. Skryshevsky, *Handbook of infrared spectroscopy of ultrathin films*, Wiley, Hoboken, U.S. (2003).
47. Z.-Q. Tian and B. Ren, *Annu. Rev. Phys. Chem.*, **55**, 197 (2004).
48. D. H. Murgida and P. Hildebrandt, *Chem. Soc. Rev.*, **37**, 937 (2008).
49. E. B. Hansson, M. S. Odziemkowski, and R. W. Gillham, *Corros. Sci.*, **48**, 3767 (2006).
50. R. Downs. The RRUFF project: an integrated study of the chemistry, crystallography, Raman and infrared spectroscopy of minerals. http://www.rruff.info (2006).
51. B. W. A. Sherar, P. G. Keech, and D. W. Shoesmith, *Corros. Sci.*, **66**, 256 (2013).
52. M. Langumier, R. Sabot, R. Obame-Ndong, M. Jeannin, S. Sablé, and P. Refait, *Corros. Sci.*, **51**, 2694 (2009).
53. Y. El Mendili, B. Minisini, A. Abdelouas, and J.-F. Bardeau, *RSC Adv.*, **4**, 25827 (2014).
54. M. Hanesch, *Geophys. J. Int.*, **177**, 941 (2009).
55. A. M. Jubb and H. C. Allen, *ACS Appl. Mater. Interfaces*, **2**, 2804 (2010).
56. D. L. A. de Faria, S. Venncio Silva, and M. T. de Oliveira, *J. Raman Spectrosc.*, **28**, 873 (1997).
57. I. Díez-Pérez, F. Sanz, and P. Gorostiza, *Curr. Opin. Solid State Mater. Sci.*, **10**, 144 (2006).
58. C. Toparli, A. Sarfraz, and A. Erbe, *Phys. Chem. Chem. Phys.*, **17**, 31670 (2015).
59. *NACE Standard TM0177-2005: Laboratory Testing of Metals for Resistance to Sulfide Stress Cracking and Stress Corrosion Cracking in H_2S Environments*. NACE International, Houston, TX, USA (2005).
60. S. Yamaguchi and T. Moori, *J. Electrochem. Soc.*, **119**, 1062 (1972).
61. L. Bellot-Gurlet, D. Neff, S. Reguer, J. Monnier, M. Saheb, and P. Dillmann, *J. Nano Res.*, **8**, 147 (2009).
62. A. Erbe, A. Sarfraz, C. Toparli, K. Schwenzfeier, and F. Niu, Optical absorption spectroscopy at interfaces. In and P. R. Lang and Y. Liu (Eds.), *Soft Matter at Aqueous Interfaces, Lect. Notes Phys.*, vol. 917, pp. 459–490. Springer, Cham, Switzerland (2016).
63. B. Sherar, P. Keech, and D. Shoesmith, *Corrosion Science*, **77**, 257 (2013).
64. M. Uda, *Z. Anorg. Allg. Chem.*, **361**, 94 (1968).
65. A. R. Lennie, S. A. T. Redfern, P. E. Champness, C. P. Stoddart, and P. F. Schofield, *Am. Miner.*, **82**, 302 (1997).
66. M. Mullet, S. Boursiquot, M. Abdelmoula, J.-M. Genin, and J.-J. Ehrhardt, *Geochim. Cosmochim. Acta*, **66**, 829 (2002).
67. E. Kroumova, M. Aroyo, J. Perez-Mato, A. Kirov, C. Capillas, S. Ivantchev, and H. Wondratschek, *Phase Transitions*, **76**, 155 (2003).
68. J. Geurts, S. Rau, W. Richter, and F. Schmitte, *Thin Solid Films*, **121**, 217 (1984).
69. J. Vigouroux, G. Calvarin, and E. Husson, *J. Solid State Chem.*, **45**, 343 (1982).
70. T.-L. Xia, D. Hou, S. C. Zhao, A. M. Zhang, G. F. Chen, J. L. Luo, N. L. Wang, J. H. Wei, Z.-Y. Lu, and Q. M. Zhang, *Phys. Rev. B*, **79**, 140510 (2009).
71. V. Gnezdilov, Y. G. Pashkevich, P. Lemmens, D. Wulferding, T. Shevtsova, A. Gusev, D. Chareev, and A. Vasiliev, *Phys. Rev. B*, **87**, 144508 (2013).
72. V. G. Hadjiev, M. N. Iliev, K. Sasmal, Y.-Y. Sun, and C. W. Chu, *Phys. Rev. B*, **77**, 220505 (2008).
73. Y. Y. Tay, T. T. Tan, M. H. Liang, F. Boey, and S. Li, *Appl. Phys. Lett.*, **93**, 111903 (2008).
74. Y. Chen, P. Schneider, B.-J. Liu, S. Borodin, B. Ren, and A. Erbe, *Phys. Chem. Chem. Phys.*, **15**, 9812 (2013).
75. A. Boughriet, R. Figueiredo, J. Laureyns, and P. Recourt, *J. Chem. Soc., Faraday Trans.*, **93**, 3209 (1997).
76. P. Colomban, S. Cherifi, and G. Despert, *J. Raman Spectrosc.*, **39**, 881 (2008).
77. M. K. Nieuwoudt, J. D. Comins, and I. Cukrowski, *J. Raman Spectrosc.*, **42**, 1335 (2011).
78. C. Avril, V. Malavergne, R. Caracas, B. Zanda, B. Reynard, E. Charon, E. Bobocioiu, F. Brunet, S. Borensztajn, S. Pont, M. Tarrida, and F. Guyot, *Meteorit. Planet. Sci.*, **48**, 1415 (2013).